Medium-range imperfect order determining the slow β-relaxation in metallic glasses

Qiang Luo[1†], Liliang Shao[1,2,3†], Lin Xue[4], Jingxian Cui[1], Qianzi Yang[1], Junpeng Wang[1], Haibo Ke[2], Baolong Shen[1*] and Weihua Wang[2,3]

ABSTRACT Secondary (slow β) relaxation and structural heterogeneity are crucial in several critical unresolved issues in metallic glasses (MGs). However, their intrinsic correlations and composition dependence are not established despite extensive work for decades. In this work, we modulated the secondary relaxation and structural heterogeneity of Dy-based bulk MGs by microalloying different metalloids (B, C, N, and Si) and demonstrated the atomic-scale mechanism. We shed light on the effects of enthalpy of mixing, degree of elastic heterogeneity on the micrometer scale, intensity of interaction, and imperfect orders (IPOs) on β-relaxation dynamics. We revealed that both the obviousness/intensity of the shoulder and the activation energy for β-relaxation are closely associated with the fraction of medium-range IPO. This shows that the cooperative string-like atomic rearrangements considered as the structural origin in terms of the first-order transition theory probably occur in soft medium-range structures (or defects) with IPO. In addition, the intensity of interaction between Dy and metalloid elements is found to play a crucial role in the formation of medium-range IPO. This work offers new insights into the longstanding mystery regarding the atomic mechanism of β-relaxation and shows significance for tuning the properties of MGs.

Keywords: β-relaxation, structural heterogeneity, metallic glass, imperfect order

INTRODUCTION

Glass is one of the most important materials that has promoted the development of modern civilization. Although glass has been used by mankind for millennia, its glassy structure and relaxation dynamics remain longstanding challenges in condensed matter physics and materials science [1–4], which originate from its complex structural and dynamic heterogeneity. Metallic glasses (MGs), which are relatively simple among different kinds of glasses, have a metallic bonding nature and lack of angle jump and intramolecular degree of freedom, which endows them with many unique and outstanding properties and makes them ideal systems for exploring the fundamental physical mechanism of glass formation and relaxation dynamics on the atomic scale [5–8].

Prepared by quenching metallic melts through the glass transition, MGs have no long-range order but considerable diversity in short- to medium-range orders [5–7]. MGs exhibit relaxation dynamics over a wide range of timescales, including α-relaxation, β-relaxation, γ-relaxation, and boson peak dynamics [9–14]. On this subject, slow β-relaxation (Johari-Goldstein β-relaxation) [15,16], intrinsic to almost all kinds of glasses, is of particular significance because it serves as the precursor of α-relaxation and correlates with many fundamental issues in glassy/liquid physics, such as diffusion, physical aging, crystallization, and fragile-to-strong dynamical transition of liquid [9,16–19]. Furthermore, it has been found that β-relaxation and shear transformation zones have almost the same activation energy, demonstrating a common structural origin [20]. Experimentally, the correlation between β-relaxation and the fraction of liquid-like zones and the distribution of flow units have also been reported [14,15,21,22]. Generally, a correlation between β-relaxation and nanoscale spatial heterogeneity exists [23,24]. Despite the intrinsic feature of spatial heterogeneity of MGs, it is not fully understood with sufficient atomic structural details why distinct relaxation behaviors with pronounced peaks, shoulders, or excess wings are observed in different systems [25–27]. Theoretically, the microscopic origin of β-relaxation remains under intense debate even in MGs [2,28–32].

In this work, rather than exploring a series of MGs with significant composition differences, minor additions (⩽ 1 at%) are employed to tune the spatial heterogeneity and β-relaxation, which can considerably simplify the exploration of the composition effect (where the content effect can be largely ignored). By dynamic mechanical, nanoindentation, and structural tests, we intend to shed new light on the following unexplored or not fully comprehended questions: What are the effects of minute changes in composition on the elastic and structural heterogeneity of MGs on different length scales? How does structural heterogeneity correlate with β-relaxation? What type of struc-

[1] School of Materials Science and Engineering, Jiangsu Key Laboratory of Advanced Metallic Materials, Southeast University, Nanjing 211189, China
[2] Songshan Lake Materials Laboratory, Dongguan 523808, China
[3] Institute of Physics, Chinese Academy of Sciences, Beijing 100190, China
[4] College of Mechanics and Materials, Hohai University, Nanjing 211100, China
† These authors contributed equally to this work.
* Corresponding author (email: blshen@seu.edu.cn)

tural motif presents cooperative string-like excitation (in the random first-order transition theory) and thus determines the intensity and activation energy of β-relaxation?

MATERIALS AND METHODS

Sample preparation
Master alloys were synthesized by arc-melting a mixture of raw metals under a Ti-gathered high-purity argon atmosphere. Each ingot was melted five times to ensure chemical homogeneity. The purity of the Dy element is higher than 99.9%, and those of Al, Co, and metalloid elements (B, C, and Si) are no less than 99.99%. The N element introduction was conducted by arc-melting the AlN compound (purity > 99.99%). Bulk metallic glass (BMG) samples were fabricated by copper mold casting.

XRD and TEM
The amorphous structure of the BMGs was studied by X-ray diffraction (XRD) and high-resolution transmission electron microscopy TEM (HRTEM). Samples for TEM studies were prepared by mechanical polishing and ion milling (PIPS 691, Gatan) at 3.0 keV and cooled with liquid nitrogen.

DSC experiments
Differential scanning calorimetry (DSC, NETZSCH 404 F3) experiments were conducted at a heating rate of 20 K min^{-1} to determine the glass transition temperature (T_g) and crystallization temperature (T_x).

Nanoindentation
Nanoindentation tests were carried out using a Hysitron TI 980 TriboIndenter with a standard Berkovich diamond indenter. For the mapping experiment, a loading rate of 100 mN s^{-1} was used, and the maximum load was 10 mN. For each sample, 14 × 14 points were measured for the distribution analysis of the reduced modulus and elastic heterogeneity. Creep measurements were performed by loading the sample at a loading rate of 30 mN s^{-1} to a maximum load of 50 mN, then a holding period of 180 s, and finally unloaded at 30 mN s^{-1}. Six independent measurements were conducted for each sample.

DMA experiments
The specimens cut from cylindrical BMG samples were mechanically polished mirror-like on one side before nanoindentation measurement. Relaxation behaviors were characterized by dynamical mechanical analysis (DMA, TA 850) with a constant heating rate of 2 K min^{-1} at driving frequencies of 1, 2, 5, and 10 Hz. Rectangular specimens with dimensions of 30 mm (length) × 2 mm (width) × 1 mm (thickness) were gripped to an oscillating system and subjected to sinusoidal single cantilever-bending strains with a limited amplitude of 15 μm.

RESULTS AND DISCUSSION
The Dy-based BMGs were selected as the model system because they have well-resolved β-relaxation peaks or shoulders and good glass-forming ability (GFA) [14]. The minor addition of metalloid elements B, C, N, and Si, with smaller atomic radii (compared with that of Dy) and a large negative enthalpy of mixing with Dy (shown in Fig. 1a) was adopted to tune the structural heterogeneity and relaxation behavior. Based on the coupling model, strong interactions originating from this large

negative enthalpy are beneficial for pronounced β-relaxation [33]. A large negative enthalpy is also favorable for glass formation [14]. The prepared BMGs, $Dy_{55}Co_{20}Al_{25}$, $Dy_{55}Co_{20}Al_{24.5}B_{0.5}$, $Dy_{55}Co_{20}Al_{24.5}C_{0.5}$, $Dy_{55}Co_{20}Al_{24.8}N_{0.2}$, and $Dy_{55}Co_{20}Al_{24}Si_1$, are denoted as DyCoAl, DyB0.5, DyC0.5, DyN0.2, and DySi1, respectively. With a minor addition of metalloids, the GFA of Dy-based BMGs was enhanced significantly, as shown in Fig. 1b, accompanied by variations in thermal properties (Fig. S1 and Table S1). From our previous studies, the improvement in GFA can be attributed to the enhanced stability of the metallic melt and the fragile-to-strong transition of the supercooled liquid resulting from the distinct change in medium-range order [34,35]. The main objective of this work is to reveal the variation of structural/elastic heterogeneity on different length scales and relaxation behavior with a minor addition of metalloid elements.

The dynamic relaxation behaviors of the Dy-based BMGs were first investigated by DMA. The relaxation spectra of the temperature dependence of the storage (E') and loss moduli (E'') at 1 Hz are displayed in Fig. 2a for the five BMGs. The E'' curves of all Dy-based BMGs exhibit pronounced β-relaxation shoulders around 400–550 K, followed by sharp α-relaxation peaks at ~650 K. Correspondingly, the E' curves present a shallow and deep minimum around the β- and α-relaxation peaks of E''. The relaxation spectra at frequencies of 1, 2, 5, and 10 Hz were further collected. With increasing frequency, the β-relaxation shoulder moves to higher temperatures, as shown typically for the DySi1 BMG in Fig. 2b. The activation energy ($E_β$) of β-relaxation determined from the Arrhenius plots in Fig. 2c for the BMGs with different metalloids is plotted in Fig. 2d. An evident change in $E_β$ upon microalloying is found. To determine the obviousness of β-relaxation in the dynamical mechanical spectrum, the parameter $∠A$ defined in Ref. [36] was also determined and is shown in Fig. 2d. The angle $∠A$ increases with the addition of B, C, and N and decreases slightly with the addition of Si, indicating a similar alloying element dependence to $E_β$.

Because β-relaxation correlates well with structural/dynamical heterogeneities and defects, such as liquid-like regions, flow units, and shear transformation zones [4,20–24], we further examine the elastic and structural heterogeneities on different length scales (micrometer and nanometer scales) as well as stress-induced relaxation by the nanoindentation method, from which the relaxation spectra are recorded. Nanoindentation experiments at an array of 14 × 14 sites were performed for each BMG sample to detect the variation of elastic heterogeneity upon minor addition (Fig. S2). Typical two-dimensionl (2D) maps of the reduced elastic moduli (E_r) of the DyCoAl and DySi1 BMGs are exhibited in Fig. 3a, b, showing a clear spatial fluctuation of the elastic properties. Some islands with low E_r are surrounded by a continuous zone with medium or high E_r. A typical distribution of the normalized E_r obtained from the 2D map of DyCoAl is displayed in Fig. 3c and the variation of the average E_r with composition is shown in Fig. S3. The full width at half-maxima (FWHMs) of the distribution curves are 4.3%, 1.7%, 4.8%, 3.5%, and 2.8% for the DyCoAl, DyB0.5, DyC0.5, DyN0.2, and DySi1 BMGs, respectively (Fig. 3d), showing an evident change in elastic heterogeneity. The addition of the C element increases the degree of elastic heterogeneity, but the addition of the other three elements decreases it. No clear correlation between the degree of heterogeneity on the micrometer scale (in terms of FWHM) and $E_β$ (or $∠A$) is observed. This suggests that heterogeneity on a smaller length scale dominates the variation
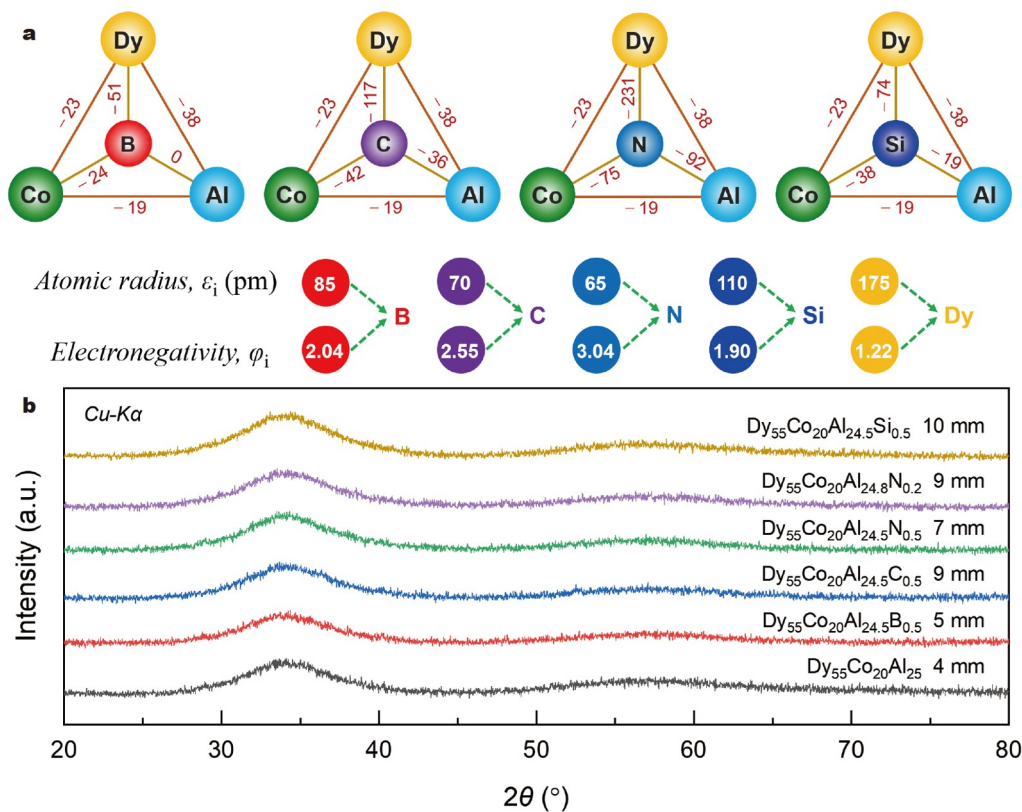
Figure 1 (a) Enthalpy of mixing (ΔH_{mix}), atomic radius (ε_i), and electronegativity (φ_i) for the studied Dy-based BMGs. (b) XRD patterns for the Dy-based BMG samples with the critical diameter.
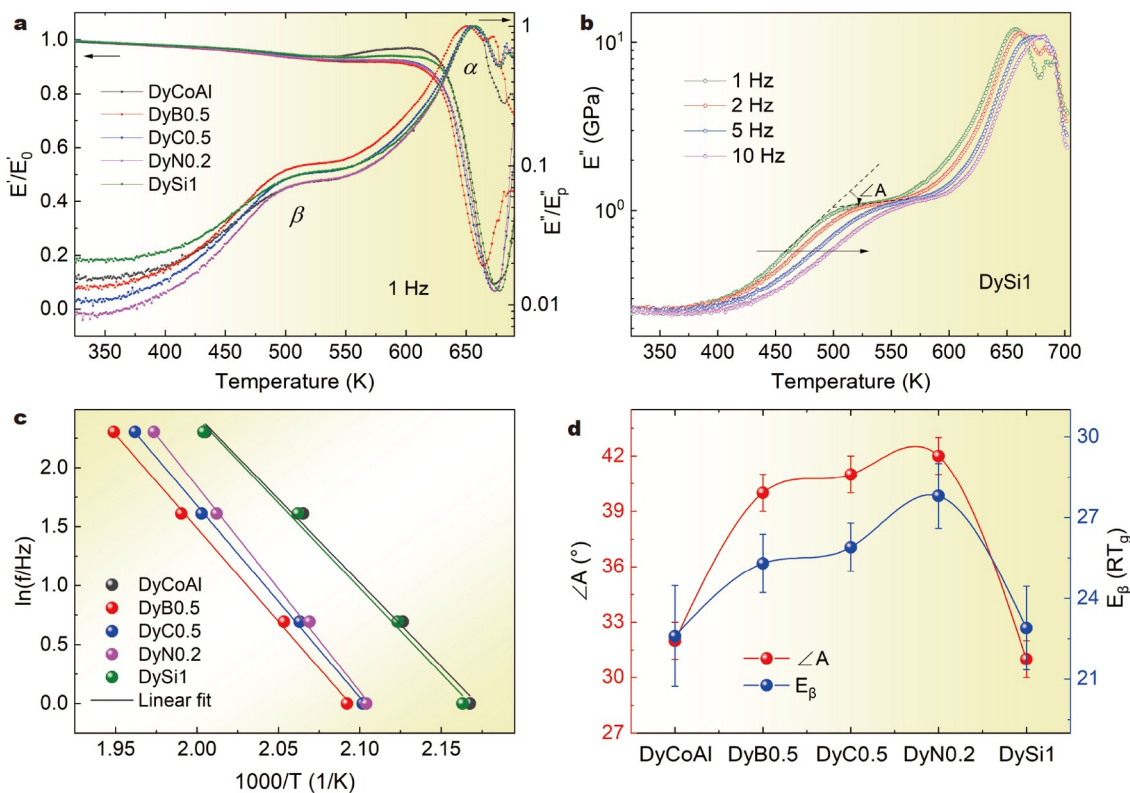
Figure 2 (a) Temperature dependence of the storage (E') and loss moduli (E'') at a heating rate of 2 K min^{-1} for the DyCoAl, DyB0.5, DyC0.5, DyN0.2, and DySi1 BMGs. (b) Evolution of E'' with temperature at different driving frequencies for the DySi1 BMG. (c) Arrhenius plots of $\ln f$ versus $1000/T_\beta$ for the Dy-based BMGs. (d) Activation energy of E_β and $\angle A$ for the Dy-based BMGs.
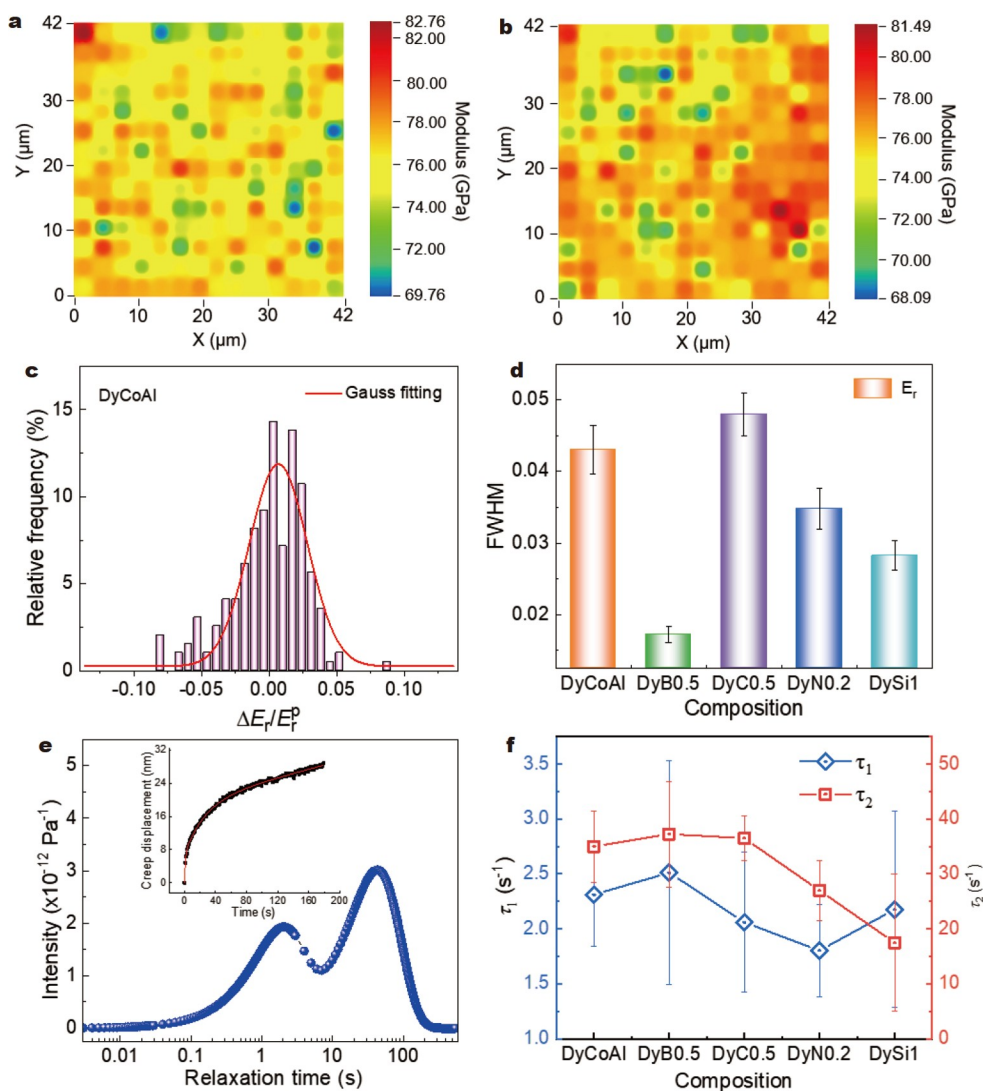
Figure 3 2D maps of the E_r of the (a) DyCoAl and (b) DySi1 BMGs. (c) Distribution of E_r for the DyCoAl BMG. (d) FWHM of the E_r distributions of the Dy-based BMGs. (e) Relaxation spectrum of the DyCoAl BMG. The inset shows the typical creep curve. (f) Variation in the positions of the first and second peaks in the relaxation spectrum with composition.

of E_β and obviousness of relaxation, and it is possible that heterogeneity on the micrometer scale has a more complex influence on β-relaxation.

Then, the relaxation time spectra from the analysis of the anelastic part of creep were collected to further detect the variation of structure defects with different sizes. The Maxwell-Voigt model, including one Maxwell unit and two Kelvin units illustrated in Fig. S4, is used to describe creep deformation [37–40]. A typical creep curve under the indentation process and its fitting by the Maxwell-Voigt model is presented in the inset of Fig. 3e for the DyCoAl BMG. The anelastic part of the creep is analyzed considering the relaxation time spectrum, which can be determined from Refs. [38,39]:

$$L(\tau) = \left[\sum_{i=1}^{n} \left(1 + \frac{t}{\tau_i}\right) \frac{h_i}{\tau_i} e^{-\frac{t}{\tau_i}} \right] \frac{A_0}{P_0 h_{in}} t \Big|_{t=2\tau}, \quad (1)$$

where L is the spectrum intensity, t is the holding time, h_i is the indentation depth, and τ_i is the characteristic relaxation time of

the i-th anelastic Kelvin unit, n is equal to 2, and A_0/P_0 is the inverse of hardness. From Fig. 3e, two separate relaxation peaks with characteristic relaxation times τ_1 and τ_2 are observed in the relaxation spectrum. It has been suggested that the first (τ_1) and second (τ_2) peaks are ascribed to activated defects with smaller and larger sizes, respectively [38,39]. From Fig. 3f, τ_1 and τ_2 show slightly different composition dependences, which may be associated with variation in the degree of heterogeneity. Fig. 3f further implies that microalloying changes the distribution of the size of activated defects during creep deformation: the addition of the B element tends to increase the size of the smaller activated defects (corresponding to τ_1) during creep deformation, but the addition of the N or C element tends to decrease it. The variation in defect distribution should influence β-relaxation, which remains elusive at present.

Subsequently, the local structure of BMG samples on atomic and nanometer scales was further characterized by TEM to determine the structural motif responsible for β-relaxation. Three representative HRTEM images of the DyCoAl, DyC0.5,

and DyN0.2 BMGs are presented in Fig. 4a–c, respectively, showing typical amorphous structures. Autocorrelation function (ACF) analysis was then conducted to determine the local structure orders on a scale of 1–2 nm [34,41,42]. The square region marked in the HRTEM image is divided into 100 segments, and the size of each cell is 1.98 nm × 1.98 nm. Note that ~2 nm is the typical length scale of the medium-range order of MGs [43]. The corresponding ACF arrays for the DyCoAl, DyC0.5, and DyN0.2 BMGs are shown in Fig. 4d–f, respectively, and those of the other two BMGs are shown in Figs S5 and S6. Some cells in the maps present clear fringe-like patterns, as marked by red squares, which are defined as medium-range imperfect order (IPO) or crystal-like order in some publications and are easy to distinguish from other regions with typical disordered structures (Fig. S7) [34]. The fraction of clusters with IPO (F_c) was thus calculated to explore the effect of microalloying on the local structure of BMGs. From Fig. 4d, the F_c of the DyCoAl BMG is 7.3% ± 0.5%. After microalloying the metalloid elements, more clusters with IPO can be observed, as shown in Fig. 4e and f. For instance, the F_c of DyN0.2 BMG is 14.7% ± 0.9%, which is approximately twice larger than that of the DyCoAl BMG. Strikingly, the variation of F_c with the metalloids (Fig. 5a) resembles that of E_β (Fig. 2d), demonstrating that β-relaxation correlates well with the structural motif with IPO.

To shed light on the correlation between F_c and E_β, we analyzed the chemical influence on the β-relaxation and formation of clusters with IPO. β-relaxation is associated with the magnitude and fluctuations of chemical interactions [27]. The mean chemical affinity ΔH_{mix} of the alloy system is then calculated by using the weighted average approach ($\Delta H_{mix} = 4 \sum_{A \neq B} \Delta H_{AB}^{mix} c_A c_B$) (where c_A and c_B are the molar percentages of elements A and B, respectively) [44] and is shown in Fig. 5a. It is evident that ΔH_{mix} decreases after metalloid

addition, especially for C, N, and Si. The variation of ΔH_{mix} and F_c upon metalloid addition indicates that a large $-\Delta H_{mix}$ may be beneficial for the formation of clusters with IPO. However, ΔH_{mix} cannot predict the accurate variation of E_β and F_c. For instance, although the E_β and F_c values for the C, N, and Si-microalloying BMGs are different, their ΔH_{mix} values are almost the same. In addition, we find that the distribution of chemical interactions cannot interpret the minor addition effect in these Dy-based BMGs showing pronounced β-relaxations either. For example, although the addition of B causes significant fluctuations in the enthalpy of mixing (ΔH_{AB}^{mix}) of the atomic pairs (Fig. 1), the DyB0.5 BMG shows increased $\angle A$ of the β-relaxation. Accordingly, the distinctions of relaxation behaviors such as E_β and $\angle A$ upon minor addition cannot be well demonstrated based only on the ΔH_{mix} and fluctuations of chemical interactions.

We further consider the intensity of interaction (W_{AB}) defined (based on the Darken-Gurry theory) as $W_{AB} = \left(\frac{\Delta \varepsilon_{AB}}{0.15}\right)^2 + \left(\frac{\Delta \varphi_{AB}}{0.4}\right)^2$, where $\Delta \varepsilon_{AB}$ is the difference in atomic radius and $\Delta \varphi_{AB}$ is the difference in electronegativity, reflecting the bonding nature between two atoms associated with the compound-forming tendency [45,46]. Here, the W_{AB} between Dy and the metalloid elements is calculated (Fig. 5a). For the DyCoAl BMG, the RE-containing clusters serve as the primary structural units, and the evaluated coordination number of the RE-Al pair in RE-TM (transition metal)-Al MGs is approximately 16 [47,48]. Thus, the W_{AB} between Dy and Al is utilized for comparison. Interestingly, W_{AB} shows the same variation trend with F_c (or E_β) as metalloids are changed, although the slight difference in metalloid content is not considered in the definition of W_{AB}. Thus, the W_{AB} between the principal and microalloying elements can be considered as a simple parameter to characterize F_c for different microalloying
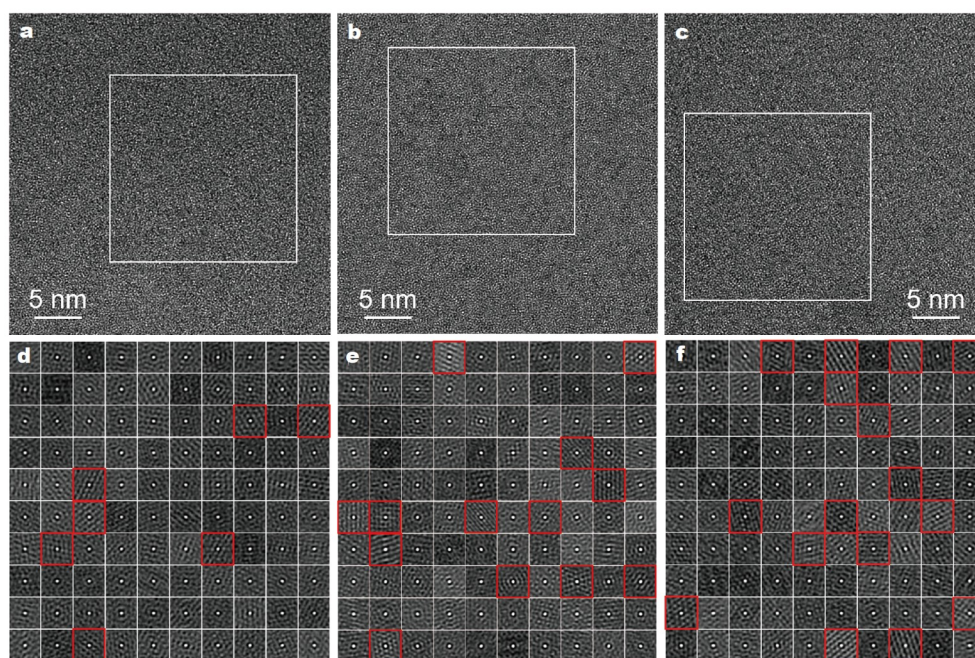
Figure 4 HRTEM images of the (a) DyCoAl, (b) DyC0.5, and (c) DyN0.2 BMG samples used in the DMA test. Corresponding autocorrelation segments of the selected square areas in (a–c) for the (d) DyCoAl, (e) DyC0.5, and (f) DyN0.2 BMGs.
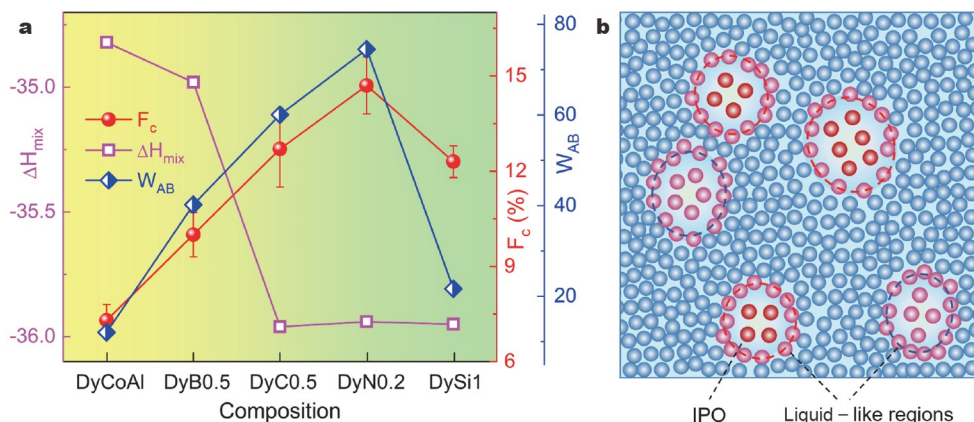
Figure 5 (a) Fraction of clusters with IPO (F_c), ΔH_{mix}, and intensity of interaction (W_{AB}) between Dy and metalloids for the DyCoAl, DyB0.5, DyC0.5, DyN0.2, and DySi1 BMG samples. (b) Schematic illustration of the atomic structures of IPOs and liquid-like regions. The blue and purple balls are atoms in the solid-like and liquid-like regions, respectively, and the reddish-brown balls are clusters with IPO in the liquid-like regions.

systems. The effectiveness is due to the comprehensive consideration of the electronegative, atomic radius, and enthalpy of mixing in W_{AB}. Figs 5a and 2d illustrate that the correlation between β-relaxation and the clusters with IPO is associated with the interaction between the principal and microalloying elements.

A recent theoretical work correlates β-relaxation with the excitations of string-like configurations, where a group of atoms moves back and forth cooperatively and reversibly like a string [30]. Subsequent molecular dynamics simulations for a Lennard-Jones glass and a model MG have supported this mechanism [49]. By simulation on a microsecond time scale, it was found that the most probable time of string-like motions is accordant with the β-relaxation time [50]. The close relationship between F_c and E_β and $\angle A$ observed here suggests that the excitation of string-like movement primarily takes place in these regions with IPO. This is reasonable because the regions with IPO have imperfect translational symmetry (with a higher degree of geometrical frustration) and comparable magnitudes of interactions among the constituting atoms, which are favorable for activating a cooperative string-like motion of the β-relaxation event. Instead, regions with large fluctuations between certain atomic pairs or with wholly disordered structures tend to break the cooperative and reversible string-like motions. Therefore, the increase in F_c after microalloying can promote the excitation of string-like motifs for β-relaxation, resulting in a more pronounced shoulder in the metalloid-doped BMGs. Then, we discuss why a larger F_c of the metalloid-doped BMG contributes to a higher E_β. Despite the presence of the IPO on the ~2 nm scale, the amorphous structure is retained, and typical nanocrystals are not observed. The limited growth of the clusters with IPO shows the presence of some stable pinning clusters (probably icosahedral-like) around them. These pinning clusters hinder the growth of clusters with IPO. A larger F_c refers to denser pinning clusters as well, which makes the activation of β-relaxation more difficult and thus leads to a larger E_β. A similar mechanism works in the microalloying effect on the GFA of Cu-, Dy-, and Gd-based BMGs [34,35,51]. The improvement of the GFA of these BMGs with a minor addition of Si or Y was associated with an increasing fraction of clusters with IPO. It has been suggested that clusters with IPO cannot grow due to the pinning effect of the surrounding icosahedron-like clusters on

the one hand and decreases the thermodynamic driving force for crystallization on the other hand [51]. Although other factors may affect the β-relaxation, this work confirms the significant effect of atomic defects with IPO on β-relaxation.

Finally, we emphasize that the medium-range IPO structure plays a critical role in the glass dynamics, nanocrystallization, glass formation, and deformation of MGs [52–56]. Such a role is similar to that of defects (i.e., some lattice points that deviate from the regular geometrical arrangement of the atoms) in influencing the properties of a crystalline solid. For instance, in MG liquids with an abnormal liquid-liquid transition, it was found that the MG prepared by high-temperature liquid has less IPO than that by low-temperature liquid [56]. In particular, in an Fe-based BMG with large plasticity, homogeneously dispersed clusters (1–1.5 nm) with IPO are observed, which are responsible for the start-and-stop mechanism of shear transformation zones [52]. In FeNi-based and Co-based BMGs, improved plasticity was found to correlate with improved structural heterogeneity with the formation of IPO structures [53,54]. Because the activation of the structural units (shear transformation zones) of plastic deformations correlates closely with β-relaxation in MGs [11], the above correlation between IPO structures and plasticity gives further evidence for IPO as the underlying structural origin of β-relaxation in MGs.

CONCLUSIONS

To sum up, we investigated the effect of microalloying ($\leqslant 1$ at%) on β-relaxation and spatial heterogeneity on different length scales. A direct relationship between β-relaxation and the degree of heterogeneity on the micrometer scale (the FWHM of the E_r distributions) or the mean chemical affinity or fluctuations in the enthalpy of mixing was not observed. Instead, both the obviousness of the shoulder peak and activation energy for β-relaxation are well linked to the fraction of medium-range structures/defects with IPO and the intensity of interaction W_{AB}. This means that cooperative string-like excitations most probably occur in regions with IPO. Note that many experimental results suggest the mechanism of local arrangements in loosely packed regions for β-relaxation [20–22,57]. This implies that medium-range structures/defects with IPO contributing to the β-relaxation are relatively loose (due to the high geometric frustration) or in liquid-like regions to aid in cooperative string-

like movements (Fig. 5b). It was experimentally revealed by angstrom-beam electron diffraction and scanning TEM that the lower-density regions in a Zr-Cu-Al MG contained IPO [58]. In addition, a recent simulation study stated that string-like motions are produced in a relatively loose environment in the $Al_{90}Sm_{10}$ MG with pronounced β-relaxation [59]. These studies corroborate our arguments that nanostructures with IPO in the liquid-like regions dominate β-relaxation in the Dy-based MGs. The mechanism schematized in Fig. 5b can explain why distinct β-relaxation behaviors with pronounced peaks, shoulders, and excess wings are observed in MGs, although they generally contain and may have a similar fraction of liquid-like regions. The key point lies in the fraction of medium-range structures/defects with IPO (in favor of string-like motions) in the liquid-like regions. Therefore, this work provides new insights into the atomic-scale mechanism of β-relaxation in MGs.

1 Berthier L, Ediger MD. Facets of glass physics. Phys Today, 2016, 69: 40–46

2 Lunkenheimer P, Schneider U, Brand R, et al. Glassy dynamics. Contemp Phys, 2000, 41: 15–36

3 Hu L, Yue Y. Secondary relaxation behavior in a strong glass. J Phys Chem B, 2008, 112: 9053–9057

4 Yue Y. Revealing the nature of glass by the hyperquenching-annealing-calorimetry approach. J Non-Cryst Solids-X, 2022, 14: 100099

5 Ding J, Patinet S, Falk ML, et al. Soft spots and their structural signature in a metallic glass. Proc Natl Acad Sci USA, 2014, 111: 14052–14056

6 Qiao JC, Wang Q, Pelletier JM, et al. Structural heterogeneities and mechanical behavior of amorphous alloys. Prog Mater Sci, 2019, 104: 250–329

7 Dmowski W, Iwashita T, Chuang CP, et al. Elastic heterogeneity in metallic glasses. Phys Rev Lett, 2010, 105: 205502

8 Liu C, Maaß R. Elastic fluctuations and structural heterogeneities in metallic glasses. Adv Funct Mater, 2018, 28: 1800388

9 Hu L, Yue Y. Secondary relaxation in metallic glass formers: Its correlation with the genuine Johari-Goldstein relaxation. J Phys Chem C, 2009, 113: 15001–15006

10 Wang WH. Dynamic relaxations and relaxation-property relationships in metallic glasses. Prog Mater Sci, 2019, 106: 100561

11 Yu HB, Shen X, Wang Z, et al. Tensile plasticity in metallic glasses with pronounced β relaxations. Phys Rev Lett, 2012, 108: 015504

12 Wang Q, Liu JJ, Ye YF, et al. Universal secondary relaxation and unusual brittle-to-ductile transition in metallic glasses. Mater Today, 2017, 20: 293–300

13 Yang Y, Zeng JF, Volland A, et al. Fractal growth of the dense-packing phase in annealed metallic glass imaged by high-resolution atomic force microscopy. Acta Mater, 2012, 60: 5260–5272

14 Shao L, Xue L, Qiao J, et al. Gamma relaxation in Dy-based metallic glasses and its correlation with plasticity. Scripta Mater, 2023, 222: 115017

15 Johari GP, Goldstein M. Viscous liquids and the glass transition. II. Secondary relaxations in glasses of rigid molecules. J Chem Phys, 1970, 53: 2372–2388

16 Johari GP. Intrinsic mobility of molecular glasses. J Chem Phys, 1973, 58: 1766–1770

17 Ichitsubo T, Matsubara E, Yamamoto T, et al. Microstructure of fragile metallic glasses inferred from ultrasound-accelerated crystallization in Pd-based metallic glasses. Phys Rev Lett, 2005, 95: 245501

18 Yu HB, Samwer K, Wu Y, et al. Correlation between β relaxation and self-diffusion of the smallest constituting atoms in metallic glasses. Phys Rev Lett, 2012, 109: 095508

19 Sun Q, Zhou C, Yue Y, et al. A direct link between the fragile-to-strong transition and relaxation in supercooled liquids. J Phys Chem Lett, 2014, 5: 1170–1174

20 Yu HB, Wang WH, Bai HY, et al. Relating activation of shear transformation zones to β relaxations in metallic glasses. Phys Rev B, 2010, 81: 220201

21 Duan YJ, Zhang LT, Qiao JC, et al. Intrinsic correlation between the fraction of liquidlike zones and the β relaxation in high-entropy metallic glasses. Phys Rev Lett, 2022, 129: 175501

22 Lu Z, Shang BS, Sun YT, et al. Revealing β-relaxation mechanism based on energy distribution of flow units in metallic glass. J Chem Phys, 2016, 144: 144501

23 Wang DP, Qiao JC, Liu CT. Relating structural heterogeneity to β relaxation processes in metallic glasses. Mater Res Lett, 2019, 7: 305–311

24 Zhu F, Nguyen HK, Song SX, et al. Intrinsic correlation between β-relaxation and spatial heterogeneity in a metallic glass. Nat Commun, 2016, 7: 11516

25 Pelletier JM, Van de Moortèle B, Lu IR. Viscoelasticity and viscosity of Pd-Ni-Cu-P bulk metallic glasses. Mater Sci Eng-A, 2002, 336: 190–195

26 Hachenberg J, Samwer K. Indications for a slow β-relaxation in a fragile metallic glass. J Non-Cryst Solids, 2006, 352: 5110–5113

27 Yu HB, Samwer K, Wang WH, et al. Chemical influence on β-relaxations and the formation of molecule-like metallic glasses. Nat Commun, 2013, 4: 2204

28 Johari GP. Localized molecular motions of β-relaxation and its energy landscape. J Non-Cryst Solids, 2002, 307-310: 317–325

29 Tanaka H. Two-order-parameter model of the liquid-glass transition. III. Universal patterns of relaxations in glass-forming liquids. J Non-Cryst Solids, 2005, 351: 3396–3413

30 Stevenson JD, Wolynes PG. A universal origin for secondary relaxations in supercooled liquids and structural glasses. Nat Phys, 2010, 6: 62–68

31 Capaccioli S, Paluch M, Prevosto D, et al. Many-body nature of relaxation processes in glass-forming systems. J Phys Chem Lett, 2012, 3: 735–743

32 Dixon PK, Wu L, Nagel SR, et al. Scaling in the relaxation of supercooled liquids. Phys Rev Lett, 1990, 65: 1108–1111

33 Ngai KL, Paluch M. Classification of secondary relaxation in glass-formers based on dynamic properties. J Chem Phys, 2004, 120: 857–873

34 Xue L, Shao L, Luo Q, et al. Liquid dynamics and glass formation of $Gd_{55}Co_{20}Al_{25}$ metallic glass with minor Si addition. J Mater Sci Tech, 2021, 77: 28–37

35 Shao L, Xue L, Wang Q, et al. Effects of Si addition on glass-forming ability and crystallization behavior of DyCoAl bulk metallic glass. J Alloys Compd, 2021, 874: 159964

36 Yu HB, Wang Z, Wang WH, et al. Relation between β relaxation and fragility in LaCe-based metallic glasses. J Non-Cryst Solids, 2012, 358: 869–871

37 Taub AI, Spaepen F. Ideal elastic, anelastic and viscoelastic deformation of a metallic glass. J Mater Sci, 1981, 16: 3087–3092

38 Castellero A, Moser B, Uhlenhaut DI, et al. Room-temperature creep and structural relaxation of Mg-Cu-Y metallic glasses. Acta Mater, 2008, 56: 3777–3785

39 Yuan CC, Liu R, Pang CM, et al. Anelastic and viscoplastic deformation in a Fe-based metallic glass. J Alloys Compd, 2021, 853: 157233

40 Ketov SV, Sun YH, Nachum S, et al. Rejuvenation of metallic glasses by non-affine thermal strain. Nature, 2015, 524: 200–203

41 Luo Q, Cui J, Zhang Z, et al. Tuning nanoscale heterogeneity by non-affine thermal strain to modulate defect activation and maximize magnetocaloric effect of metallic glass. Mater Des, 2023, 225: 111500

42 Fan GY, Cowley JM. Auto-correlation analysis of high resolution electron micrographs of near-amorphous thin films. Ultramicroscopy, 1985, 17: 345–355

43 Yang Y, Zhou J, Zhu F, et al. Determining the three-dimensional atomic structure of an amorphous solid. Nature, 2021, 592: 60–64

44 Takeuchi A, Inoue A. Classification of bulk metallic glasses by atomic size difference, heat of mixing and period of constituent elements and its application to characterization of the main alloying element. Mater Trans, 2005, 46: 2817–2829

45 Kim W, Oh HS, Park ES. Manipulation of thermal and mechanical

stability by addition of multiple equiatomic rare-earth elements in Al-TM-RE metallic glasses. Intermetallics, 2017, 91: 8–15

46 Li X, Bian X, Hu L, et al. Glass transition temperature of bulk metallic glasses: A linear connection with the mixing enthalpy. J Appl Phys, 2007, 101: 103540

47 Ahn K, Louca D, Poon SJ, et al. Topological and chemical ordering induced by Ni and Nd in $Al_{87}Ni_7Nd_6$ metallic glass. Phys Rev B, 2004, 70: 224103

48 Sheng HW, Luo WK, Alamgir FM, et al. Atomic packing and short-to-medium-range order in metallic glasses. Nature, 2006, 439: 419–425

49 Cohen Y, Karmakar S, Procaccia I, et al. The nature of the β-peak in the loss modulus of amorphous solids. Euro Phys Lett, 2012, 100: 36003

50 Yu HB, Richert R, Samwer K. Structural rearrangements governing Johari-Goldstein relaxations in metallic glasses. Sci Adv, 2017, 3: e1701577

51 Wang Q, Liu CT, Yang Y, et al. The atomic-scale mechanism for the enhanced glass-forming-ability of a Cu-Zr based bulk metallic glass with minor element additions. Sci Rep, 2014, 4: 4648

52 Sarac B, Ivanov YP, Chuvilin A, et al. Origin of large plasticity and multiscale effects in iron-based metallic glasses. Nat Commun, 2018, 9: 1333

53 Zhou J, Wang Q, Zeng Q, et al. A plastic FeNi-based bulk metallic glass and its deformation behavior. J Mater Sci Tech, 2021, 76: 20–32

54 Wang Q, Zhou J, Zeng Q, et al. Ductile Co-based bulk metallic glass with superhigh strength and excellent soft magnetic properties induced by modulation of structural heterogeneity. Materialia, 2020, 9: 100561

55 Liu XJ, Chen GL, Hou HY, et al. Atomistic mechanism for nanocrystallization of metallic glasses. Acta Mater, 2008, 56: 2760–2769

56 Chu W, Shang J, Yin K, et al. Generality of abnormal viscosity drop on cooling of CuZr alloy melts and its structural origin. Acta Mater, 2020, 196: 690–703

57 Wang Z, Sun BA, Bai HY, et al. Evolution of hidden localized flow during glass-to-liquid transition in metallic glass. Nat Commun, 2014, 5: 5823

58 Zhu F, Hirata A, Liu P, et al. Correlation between local structure order and spatial heterogeneity in a metallic glass. Phys Rev Lett, 2017, 119: 215501

59 Zhou ZY, Sun Y, Gao L, et al. Fundamental links between shear transformation, β relaxation, and string-like motion in metallic glasses. Acta Mater, 2023, 246: 118701

Author contributions Luo Q, Shao L, and Shen B conceptualized this work and designed the experiments. Luo Q and Shao L analyzed the experimental data and wrote the manuscript with the input and advice from Ke H, Wang W, and Shen B. Shao L and Xue L prepared the samples, and carried out the XRD, DMA, and TEM experiments. Cui J, Yang Q, and Wang J carried out the DSC and nanoindentation experiments. All authors contributed to the general discussion.

Conflict of interest The authors declare that they have no conflict of interest.

Supplementary information Supporting data are available in the online version of the paper.

Qiang Luo received his PhD degree in condensed matter physics from the Institute of Physics, Chinese Academy of Sciences in 2008, and was a postdoctoral researcher as Humboldt scholar at the Leibniz Institute for Solid State and Materials Research Dresden, Germany, during 2009–2011. He conducted research at Tongji University from 2012 to 2017. He is currently a professor at Southeast University. His research interests focus on the structures, dynamics, properties, and applications of amorphous and nanocrystalline alloys.

Baolong Shen received his PhD degree in engineering from Himeji Institute of Technology in 1999 and was a postdoctoral researcher then an assistant professor (faculty member) at the Institute for Materials Research at Tohoku University, Japan, during 1999–2007. He conducted research at Ningbo Institute of Materials Technology and Engineering, Chinese Academy of Sciences from 2007 to 2012. He is currently the Chair Professor at Southeast University. His research interests focus on the formation, structures, properties, and applications of ferromagnetic disordered alloys.

中程尺度类晶体结构决定非晶合金慢二次弛豫

罗强[1†], 邵里良[1,2,3†], 薛琳[4], 崔静贤[1], 杨芊姿[1], 王俊鹏[1], 柯海波[2], 沈宝龙[1*], 汪卫华[2,3]

摘要 二次弛豫特别是慢β弛豫和结构不均匀性是非晶合金悬而未决的关键问题. 尽管经历了几十年的深入研究, 慢β弛豫与结构不均匀性之间的本征关联及其成分依赖性尚未建立. 本文以镝基块体非晶合金为载体, 通过微量掺杂不同类金属元素包括硼、碳、氮和硅, 实现了β弛豫的有效调控, 并且揭示了其原子尺度结构起源. 通过对比研究混合焓、弹性不均匀度、相互作用强度和不完美序结构(或类晶体结构)对β弛豫的影响, 发现β弛豫强度与中程类晶体结构的含量密切相关(与混合焓没有显著的对应关系), 这表明原子的链状协同运动发生在含有类晶体结构的中程序软区. 此外, 镝元素和类金属元素之间的相互作用强度对于类晶体结构的形成至关重要. 本工作对于理解β弛豫的原子结构起源和调控非晶合金性能具有重要意义.